Monthly Notices
of the
ROYAL ASTRONOMICAL SOCIETY

MNRAS **493,** 5389–5396 (2020)
Advance Access publication 2020 February 27

doi:10.1093/mnras/staa564

The soft state of the black hole transient source MAXI J1820+070: emission from the edge of the plunge region?

A. C. Fabian [1]★ D. J. Buisson,[1] P. Kosec,[1] C. S. Reynolds,[1] D. R. Wilkins [2] J. A. Tomsick,[3] D. J. Walton [1] P. Gandhi,[4] D. Altamirano,[4] Z. Arzoumanian,[5] E. M. Cackett,[6] S. Dyda,[1] J. A. Garcia,[7] K. C. Gendreau,[5] B. W. Grefenstette,[7] J. Homan,[8,9] E. Kara [10] R. M. Ludlam,[7] J. M. Miller[11] and J. F. Steiner[12]

[1]*Institute of Astronomy, Madingley Road, Cambridge CB3 0HA, UK*
[2]*Kavli Institute for Particle Astrophysics and Cosmology, Stanford University, 452 Lomita Mall, Stanford, CA 94305, USA*
[3]*Space Sciences Laboratory, 7 Gauss Way, University of California, Berkeley, CA 94720-7450, USA*
[4]*Department of Physics and Astronomy, University of Southampton, Highfield, Southampton SO17 1BJ, UK*
[5]*Astrophysics Science Division, NASA's Goddard Space Flight Center, Greenbelt, MD 20771, USA*
[6]*Department of Physics and Astronomy, Wayne State University, 666 W. Hancock Street, Detroit, MI 48201, USA*
[7]*Cahill Center for Astronomy and Astrophysics, California Institute of Technology, Pasadena, CA 91125, USA*
[8]*Eureka Scientific, Inc., 2452 Delmer Street, Oakland, CA 94602, USA*
[9]*SRON, Netherlands Institute for Space Research, Sorbonnelaan 2, NL-3584 CA Utrecht, the Netherlands*
[10]*MIT Kavli Institute for Astrophysics and Space Research, 70 Vassar Street, Cambridge, MA 02139, USA*
[11]*Department of Astronomy, University of Michigan, 1085 South University Avenue, Ann Arbor, MI 48109-1107, USA*
[12]*Center for Astrophysics, Harvard University, 60 Garden Street, Cambridge, MA 02138, USA*

Accepted 2020 February 21. Received 2020 February 19; in original form 2019 November 5

ABSTRACT

The Galactic black hole X-ray binary MAXI J1820+070 had a bright outburst in 2018 when it became the second brightest X-ray source in the sky. It was too bright for X-ray CCD instruments such as *XMM–Newton* and *Chandra*, but was well observed by photon-counting instruments such as *Neutron star Inner Composition Explorer* (*NICER*) and *Nuclear Spectroscopic Telescope Array* (*NuSTAR*). We report here on the discovery of an excess-emission component during the soft state. It is best modelled with a blackbody spectrum in addition to the regular disc emission, modelled as either `diskbb` or `kerrbb`. Its temperature varies from about 0.9 to 1.1 keV, which is about 30–80 per cent higher than the inner disc temperature of `diskbb`. Its flux varies between 4 and 12 per cent of the disc flux. Simulations of magnetized accretion discs have predicted the possibility of excess emission associated with a non-zero torque at the innermost stable circular orbit (ISCO) about the black hole, which, from other *NuSTAR* studies, lies at about 5 gravitational radii or about 60 km (for a black hole, mass is 8 $M_\odot$). In this case, the emitting region at the ISCO has a width varying between 1.3 and 4.6 km and would encompass the start of the plunge region where matter begins to fall freely into the black hole.

Key words: accretion, accretion discs – X-rays: binaries – black hole physics.

1 INTRODUCTION

On 2018 March 6, Tucker et al. (2018) discovered a new optical source from the All-Sky Automated Survey for SuperNovae project (Shappee et al. 2014) and designated it ASASSN-18ey. After 5 d, the Monitor of All-sky X-ray Image (MAXI; Matsuoka et al. 2009) on the *International Space Station* (*ISS*) detected its X-ray emission (Kawamuro et al. 2018) and classified it as a new Galactic black hole candidate MAXI J1820+070 (see Shidatsu et al. 2019 for a summary of observations, in particular of those made by MAXI). The source displayed a hard spectrum that rapidly rose to a peak flux, making it the second brightest object in the X-ray sky. It then slowly decayed in brightness while remaining in the hard state before, in 2018 June, the spectrum became soft, peaking in flux before slowly decaying again (Fig. 1). Later in 2018 September, it turned hard and continued to drop in flux. The hard–soft–hard behaviour is typical for a stellar-mass black hole binary source. The black hole nature

★ E-mail: acf@ast.cam.ac.uk

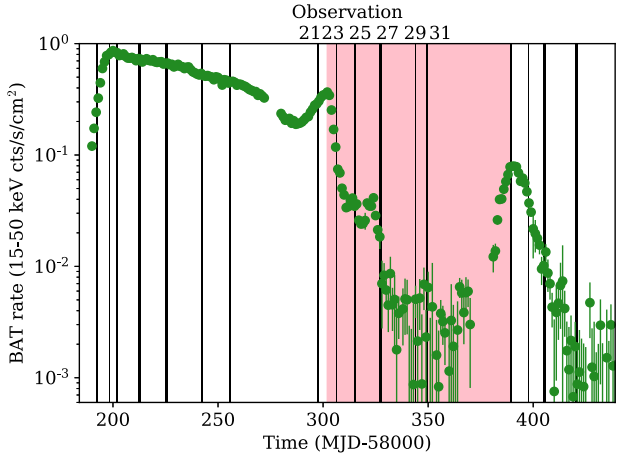

Figure 1. *Swift*-BAT light curve with *NuSTAR* observations discussed here indicated by vertical lines. The shaded region covers the soft state. The start dates and observation length and live fractions of observations 21–31 are June 28 (77 ks, 0.5), July 7 (38.1, 0.33), July 15 (43.7, 0.39), July 28 (83.3, 0.45), August 13 (26.5, 0.54), and August 19 (58.7, 0.58).

of the system has recently been confirmed by optical spectroscopy (Torres et al. 2019).

X-ray detectors on the *Neutron star Inner Composition Explorer* (*NICER*) instrument (Gendreau at al. 2016), also on the ISS, recorded incident count rates up to 50 000 counts s^{-1} in the hard state. When at 20 000 counts s^{-1}, Kara et al. (2019) found X-ray reverberation lags of a millisecond and less, confirming its status as an accreting black hole. The amplitude of the lag changed systematically during the decay from the first peak, indicating that the corona was shrinking in height. This agrees with the behaviour of X-ray spectra from the *Nuclear Spectroscopic Telescope Array* (*NuSTAR*; Buisson et al. 2019).

Here we study *NuSTAR* and *NICER* spectra from the soft sate of MAXI J1820+070. We use a *NICER* spectrum to confirm the disc blackbody nature of the emission in the energy range 0.8–7 keV and *NuSTAR* spectra from several epochs in the soft state to examine the spectrum from 3 to 78 keV. Significant excess emission found in the energy range 6–10 keV is best modelled by an additional blackbody component. It is plausibly explained as emission from the transition between the stably orbiting accretion disc and the plunge region, where matter spirals into the black hole (Hawley & Krolik 2002; Machida & Matsumoto 2003; Zhu et al. 2012).

2 THE X-RAY SPECTRA

We concentrate on five soft-state *NuSTAR* spectra, here designated as Nu23, 25, 27, 29, and 31. (They are distinguished by the last two digits in their OBSIDs.) Monitoring of the source by the hard X-ray Burst Alert Telescope (BAT) on the Neil Gehrels *Swift* satellite shows minimum flux from 2019 July 28 to September 10, during which three *NuSTAR* spectra were obtained, Nu27–31, respectively (Fig. 1). A 1.5 -ks *NICER* spectrum from July is contemporaneous with Nu29. *NuSTAR* spectra have been reduced as described in Buisson et al. (2019). The *NICER* spectrum has been analysed with response matrix version 1.02 corrected by the application of a function derived from observations of the Crab nebula (Ludlam et al. 2018).

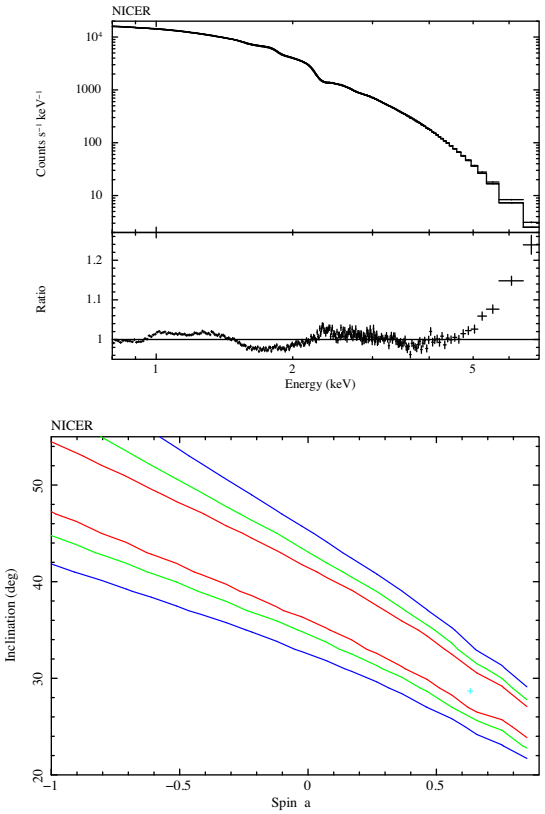

Figure 2. Top panel: *NICER* spectrum from *NuSTAR* epoch 29. Most of the residuals from 0.8 to 3 keV are instrumental. Bottom panel: allowed region using `kerrbb`. The hard-state results from Buisson et al. (2019) indicate that the spin lies between about 0 and 0.5 and inclination between 30° and 40°, which is compatible with this result.

2.1 A *NICER* soft-state spectrum

We fit the *NICER* spectrum (OBSID 1200120236) with a simple absorption model `TBNEW` applied to a `kerrbb` model, which is a fully relativistic representation of the quasi-blackbody emission expected from a thermal accretion disc (Li et al. 2005). The distance to the source is set at 3.5 kpc, as determined from *Gaia* parallax data by Gandhi et al. (2019), who derive a distance of 3.5 ± 1.5 kpc. The mass function of the binary system has been determined from optical spectroscopy by Torres et al. (2019) to be $f(M) = 5.18 \pm 0.15\,M_\odot$. They obtained an orbital inclination between 69° and 77° from the lack of a continuum eclipse and periodic changes in Hα equivalent width. This implies a black hole mass of 7–8 $M_\odot$. Buisson et al. (2019) found the inclination of the inner accretion disc to lie between 30° and 40° from relativistic reflection spectral fits to the *NuSTAR* hard-state spectra.

Our best fit is shown in Fig. 2 with the constraints on spin and inclination in the lower panel. The reduced χ^2 is 8 over the 0.8–7 keV range, which arises from known calibration inadequacies in the response files used here. Adding systematics of 1.5 per cent brings the reduced χ^2 close to unity (0.99). The level of absorption indicates a low column density of $N_{\rm H} \sim 5 \times 10^{20}\,{\rm cm}^{-2}$ and the black hole mass implied by the `kerrbb` model lies between 5 and 10 $M_\odot$. We note an excess in the spectrum above 6 keV. If the inclination of the inner disc is ∼70°, to match the optically derived orbital inclination, then we find that the spin must be close to maximally retrograde, i.e. $a < -0.95$. If, however, the inner-disc inclination is lower at 30°–40°, then the spin lies approximately

between −0.5 and +0.5. More detailed spectral fits involving the hard state and both *NICER* and *NuSTAR* will be reported elsewhere.

2.2 The *NuSTAR* spectra

2.2.1 Phenomenology and the need for an extra blackbody component

We then examine the five sets of *NuSTAR* observations that span the soft state, here designated as Nu23, Nu25, Nu27, N29, and Nu31. For comparison, we add Nu21, which is in the second rise of the hard state before the abrupt drop in BAT 14–195 keV count rate marks the beginning of the soft state. Nu23 and Nu25 have a significant BAT flux, whereas Nu27–Nu31 are faint in the BAT. The count spectra of *NuSTAR* module A[1] are plotted in Fig. 3 with the ratios of those spectra to a freely fitted `diskbb + po` model. No absorption is used as its effect is negligible at the energies of the *NuSTAR* spectra. The ratio spectrum of Nu21 (shown in black markers in Fig. 3) is typical of the hard state with a peak centred at about 6.5 keV, which corresponds to the broad iron line (Buisson et al. 2019). Spectral fits to the spectrum of Nu21 with a double corona model (epoch 8 in Buisson et al. 2019) reveal that the weak upper corona in Nu21 lies at a height of at least $100r_g$ and the coronal temperature is also high at $kT \sim 230$ keV, and the bulk of the power law is emitted close to the black hole ($<10r_g$). The disc blackbody component is detectable only below 4 keV.

In contrast, the soft-state ratio spectra Nu23–Nu31 (red through magenta in Fig. 3) are dominated by the disc blackbody spectrum up to about 10 keV. This is due principally to the disc emission becoming much stronger but also to the power-law component becoming progressively weaker. There is again a peak in the ratio spectra, but now it is much stronger and its peak shifts to almost 8 keV by Nu27 (Fig. 3)

The excess occurs where the Wien tail of the disc blackbody emission is steepest, as shown in Fig. 4. A further power law to account for this has been mimicked by the SIMPL model (Steiner et al. 2009), but it needs to be implausibly steep with a photon index $\Gamma = 7$–8. We have also briefly considered radiative transfer effects such as those responsible for the spectral correction factor commonly applied to accretion disc models. The emission is at too high an energy to be related to changes in free–free absorption within the disc.

2.2.2 Results from NuSTAR *spectral fits*

Nu21–31 have been jointly fitted with the spectral models `diskbb+bb+cutoffpl`, `ezdiskbb+bb+cutoffpl`, and `kerrbb+bb+cutoffpl`. `diskbb` and `ezdiskbb` are blackbody accretion disc models, where the first (Makishima et al. 1986) assumes a continuing torque to the inner radius and the second assumes zero torque there (Zimmerman et al. 2005). For `kerrbb`, the spin a and inclination i have been fixed at 0.2° and 34°, respectively, based on the hard-state results (Buisson et al. (2019). *Mdd* is the mass accretion rate in units of 10^{18} g s^{-1} . χ^2 for the three models (`diskbb, ezdiskbb, kerrbb`) were 8096, 8079, and 8401 for 6944, 6984, and 6945 degrees of freedom, respectively. Much of the excess χ^2 is due to the poor fit above 50 keV (Fig. 5).

[1]Just one module is used here for illustrative purposes to avoid cluttering the figure too much. Both modules A and B are used in all spectral parameter fits.

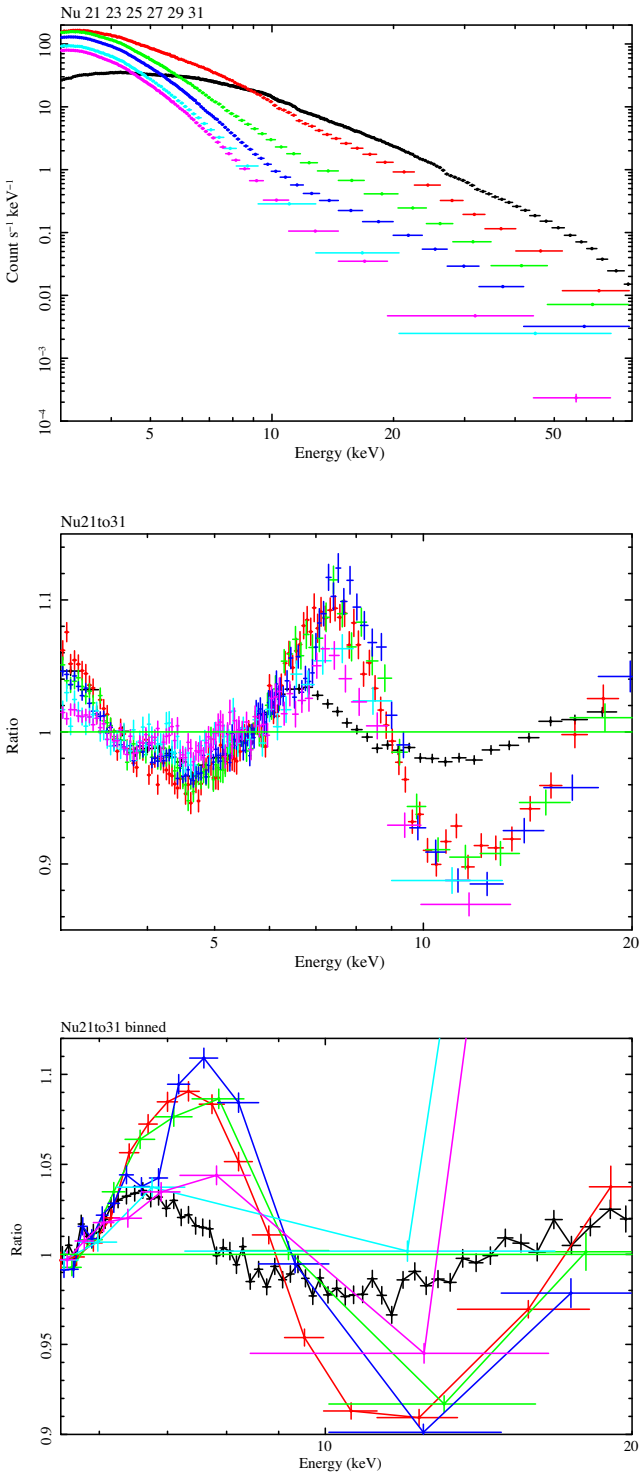

Figure 3. Top panel: *NuSTAR* module A spectra of observations 23–31 with ratios to the best-fitting power law below. The black points are from observation 21, which is on the flux rise to the soft state. Note that the black, hard-state residuals peak at 6.5 keV, whereas those in the soft state peak around 7.5 keV. For visualization purposes, the lowest panel shows a wider binning over a narrower energy range than for the middle panel. Also note that the underlying continuum, which forms the denominator of the ratio plotted here, falls very rapidly over the energy band shown.

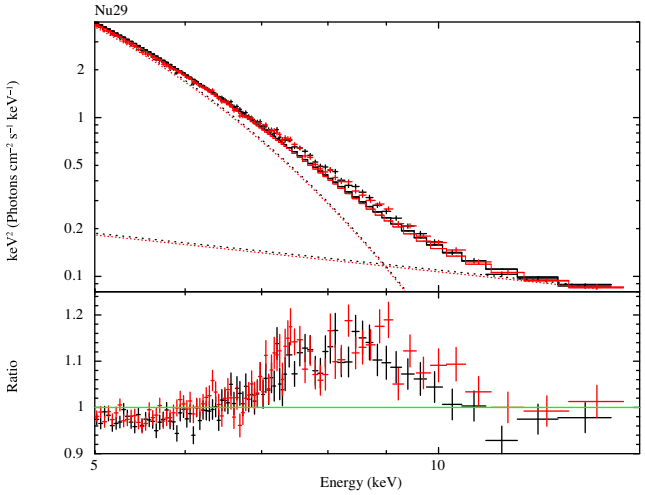

Figure 4. *NuSTAR*-unfolded spectrum from observation 29 showing the subtle nature of the excess emission in the Wien tail of kerrbb. Here a power-law continuum has been fitted to the data above 10 keV and is only for illustrative purposes as it is not the best fit in a χ^2 sense, which prefers a dip at 10 keV, as seen in Fig. 4.

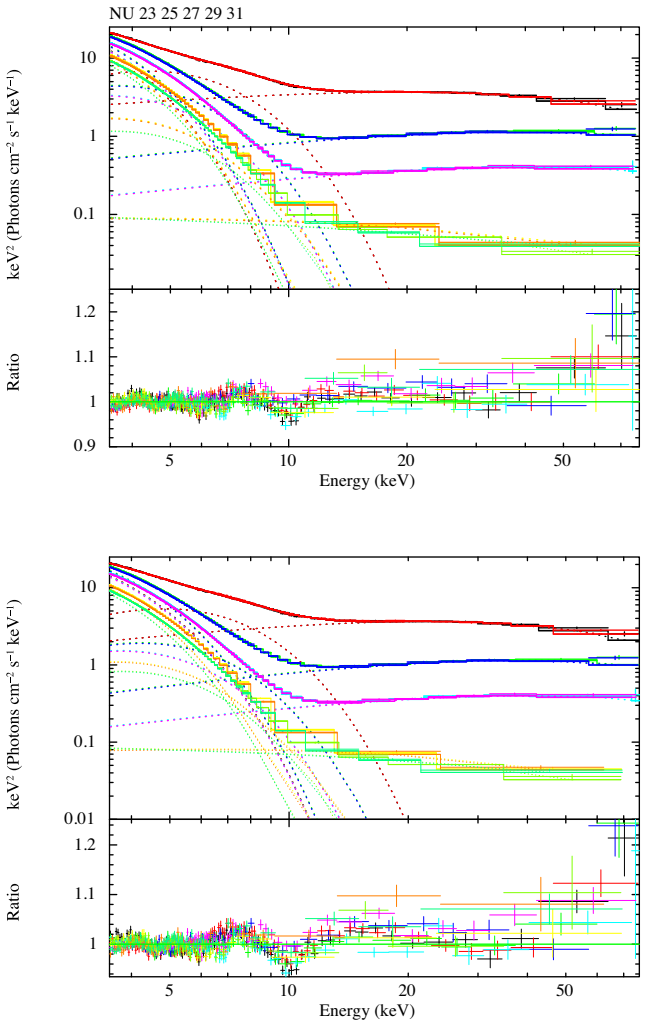

Figure 5. Top panel: Unfolded spectra of Nu23–31 using `diskbb`. Bottom panel: `kerrbb` with an extra blackbody and cut-off power-law components. The parameters are given in Tables 1 and 2.

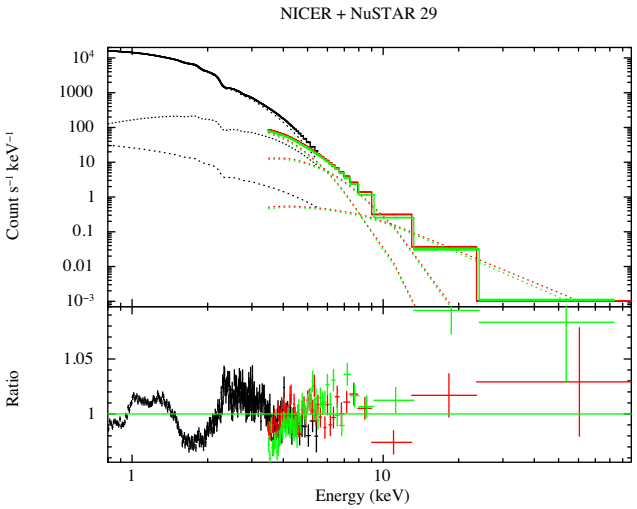

Figure 6. Joint *NICER* and *NuSTAR* fit to epoch 29 with `constant*(ezdiskbb + bb + pco)`.

The properties of the excess blackbody components are given in Tables 1 and 2. Where the disc blackbody is used, the surface area required at the source, assumed to lie at 3.5 kpc, has been estimated.[2] Assuming that the area is that of a thin ring at the innermost stable circular orbit (ISCO) lying at $5r_g$ (Buisson et al. 2019), 60 km from an 8-$M_\odot$ black hole, we find a width ΔR ranging from 4.66 ($0.4r_g$, Nu25) to 1.27 km ($0.1r_g$, Nu31), which will systematically vary as $\cos i$. The flux in the excess blackbody compared with that of the disc varies monotonically from 12 to 3.8 per cent from Nu23 to Nu31 when `diskbb` is used and 12.6 to 3.3 per cent for `kerrbb`, mostly due to changes in normalization rather than temperature. The flux in the power-law component depends on the low energy limit assumed: For 0.1 keV, it drops by about a factor of 40 in flux from 16 per cent of `diskbb` to 0.8 per cent. This disparity between the flux changes of the excess blackbody and power-law components argues against any reflection interpretation (discussed later). The extent of the variations in the blackbody does not obviously associate it directly with either the disc or the power-law component.

In Fig. 6, we show a joint fit of `constant * (ezdiskbb + bb + pco)` to the *NICER* and *NuSTAR* data from epoch 29. Again, the fit is acceptable in a χ^2 sense if 1.5 per cent systematics are included. The fit confirms that the `bb` component has a higher temperature than that of `ezdiskbb`. (This issue was ambiguous when just *NuSTAR* is used.) While `constant` is set to unity for *NuSTAR* module A, it fits to 0.43 for *NICER* due to over half the mirror modules being switched off to deal with the high count rate. The parameters for `ezdiskbb` and `bb` are similar to those listed in Table 1, and the power-law fit is changed to $\Gamma = 1.6$, $E_{\rm cut} = 25$ keV, and Norm = 5e−2.

We have also considered whether it can be due to iron emission (and absorption) as in the models by Ross & Fabian (2007). These model a slab illuminated from above by a power law and from below by a blackbody, thereby mimicking an irradiated blackbody disc. Strong Fe K features are seen when the blackbody has a temperature of 0.3 keV, but the features are weak by a temperature of 0.5 keV (fig. 6 of Ross & Fabian 2007, which shows just the radiation

[2]Relativistic blurring of a ring at $5r_g$ can lead to systematic changes in the estimated temperature of 5–10 per cent, depending on inclination.

Table 1. The best-fitting model parameters for the model `diskbb+bb+cutoffpl`. Errors are quoted at the 90 per cent confidence level. Fluxes are in units of erg cm^{-2} s^{-1} . Flux ratio is the `bb` flux divided by the `diskbb` flux. Luminosities are in units of 10^{38} erg s^{-1} .

Observation		23	25	27	29	31
Total Model	Flux (0.1–78 keV)	1.62e−7	1.30e−7	1.03e−7	7.81e−8	6.98e−8
	Luminosity	2.26	1.8	1.43	1.08	0.967
`diskbb`	$kT_{\rm in}$ (keV)	0.603 ± 0.01	0.650 ± 0.12	0.659 ± 0.01	0.651 ± 0.013	0.644 ± 0.007
	Norm	$4.45e4^{+5e3}_{-4.5e3}$	3.02e4 ± 3e3	$2.35e4^{+1.8e3}_{-1.6e3}$	$1.94e4^{+2.1e3}_{-1.7e3}$	$1.82\ e4^{+1.1e3}_{-9.7e2}$
	Flux (0.1–78 keV)	1.24e−7	1.14e−7	9.39e−8	7.35e−8	6.63e−8
`bbody`	kT (keV)	1.12 ± 0.012	0.93 ± 0.02	0.87 ± 0.014	0.89 ± 0.03	0.92 ± 0.02
	Norm	0.177 ± 0.004	0.116 ± 0.012	0.087 ± 0.01	0.045 ± 0.009	0.03 ± 0.005
	Flux (0.1–78 keV)	1.48e−8	9.76e−9	7.28e−9	3.74e−9	2.54e−9
	Area (1e12 cm^2)	12.7	17.6	17.4	8.1	4.8
	ΔR (km)	3.36	4.66	4.61	2.14	1.27
	Flux ratio	0.12	0.086	0.078	0.05	0.038
	Temp ratio	1.86	1.43	1.31	1.25	1.42
`cutoffpl`	Γ	1.6 ± 0.06	1.47 ± 0.07	1.45 ± 0.063	1.92 ± 0.03	2.14 ± 0.24
	$E_{\rm cut}$ (keV)	49.8 ± 5.5	73.8^{+18}_{-12}	74^{+17}_{-12}	36.9^{+43}_{-14}	64.6^{+114}_{-26}
	Norm	1.67 ± 0.2	0.284 ± 0.04	0.093 ± 0.012	$0.083^{+0.09}_{-0.05}$	$0.116^{+0.07}_{+0.04}$
	Flux (0.1–78 keV)	2.39e−8	6.0e−9	2.06e−9	7.97e−10	1.0e−9
	Flux (1–78 keV)	1.99e−8	5.4e−9	1.86e−9	5.0e−10	5.0e−10
`ezdiskbb`	$kT_{\rm max}$ (keV)	0.574 ± 0.01	0.615 ± 0.11	0.621 ± 0.01	0.615 ± 0.013	0.615 ± 0.007
	Norm	$9.39e3^{+1.0e3}_{-9.3e2}$	$6.6e3^{+7e2}_{-6e2}$	$5.2e3^{+3.9e2}_{-3.4e2}$	$4.24e3^{+4.6e2}_{-3.7e2}$	$3.95e3^{+2.4e2}_{-2.1e2}$
`bbody`	kT (keV)	1.12 ± 0.012	0.92 ± 0.02	0.86 ± 0.014	0.88 ± 0.03	0.91 ± 0.02
	Norm	0.177 ± 0.004	0.122 ± 0.11	0.095 ± 0.01	0.049 ± 0.01	0.033 ± 0.004

Table 2. The best-fitting model parameters for the model `kerrbb+bb+cutoffpl`.

Observation		23	25	27	29	31
`kerrbb`	*Mdd*	1.72 ± 0.13	1.92 ± 0.009	1.70 ± 0.006	1.37 ± 0.009	1.25 ± 0.005
	F(0.1–78 keV)	9.43e-8	1.045e-7	9.23e-8	7.45e-8	6.81e-8
`bbody`	kT keV	1.24 ± 0.01	1.08 ± 0.015	0.953 ± 0.009	0.937 ± 0.016	0.96 ± 0.01
	Norm	0.138 ± 0.002	5e-2 ± 0.17e-3	4e-2 ± 1.5e-3	2.9e-2 ± 1.7e-3	2.15e-2 ± 8e-4
	F(0.1–78 keV)	1.19e-8	5.06e-9	4.36 e-9	3.07e-9	2.29e-9
	Flux ratio	0.126	0.048	0.047	0.041	0.033

emerging from the slab). First, in order to measure the amplitude of any Fe K emission, we replaced the extra blackbody with a Gaussian component, centred at 6.5 keV. This gives a reasonable fit to the joint data of Nu29 but for a standard deviation of about 1.5 keV. Under this model, the excess shown in Fig. 4 represents the high-energy shoulder of the Gaussian component. The equivalent width (EW) of the Gaussian emission is almost 4 keV when measured against the power-law component alone, which we consider too strong to be plausible (see Matt, Fabian & Ross 1993; Zycki & Czerny 1994, for Fe K EW predictions).

Secondly, we tried fitting the `refbhbhi` model from Ross & Fabian (2007), which involves the whole reflection spectrum, to the joint Nu29 data. We find a reasonable fit for an inclination of 85° with an uncertainty of less than 1°. Cstat increases by about 40 if reduced to 77° in order to become consistent with the optical date. This result could imply that reflection may be involved but is not a clear answer. A major concern is that Fe K reflection features are produced by irradiation of the disc by photons near 7 keV. The flux from the power-law component at that energy varies by a factor of 41 from Nu23 to Nu31, whereas the flux of the excess component, measured as the extra blackbody, varies only by a factor of only 5.9. Unless the geometry of the irradiation changes by significant factors, we do not see how they are causally connected.

One characteristic of the spectral residuals seen in Fig. 5 is a broad dip at 10 keV, and some spectra (Nu27 and Nu31) also show a dip just below 7 keV. For the latter, ionized absorption is a likely explanation. Therefore, we have added a negative Gaussian at around 6.6 keV and an edge at about 9.2 keV. This improves the spectral fit by $\Delta\chi^2 = -35$ (Fig. 7). A separate fit with SPEX using the model `pion` reveals an ouflowing wind with a column density of 2–4 × 10^{21} cm^{-2}, outflow velocity of around 4000 km s^{-1} , and ionization parameter $\xi \sim 3000$ erg cm^{-2} s^{-1}. The fit is not improved significantly by using that model for the earlier observations Nu23, 25, or 29. We note that such outflows are common in the soft state of black hole X-ray binaries (Ponti et al. 2012), usually if they have a high inclination.

3 THE PLUNGE REGION

The additional component seen in the spectra is well explained by the addition of another blackbody, with a temperature slightly higher than that of the disc itself. The ratio of temperature of the blackbody to the inner `diskbb` temperature is between 1.25 (epoch 27) and 1.86 (epoch 23, see Table 1). It appears to be a separate component. Since temperatures increase inwards in the disc, we associate it with the innermost part of the disc and with the start of the plunge region.

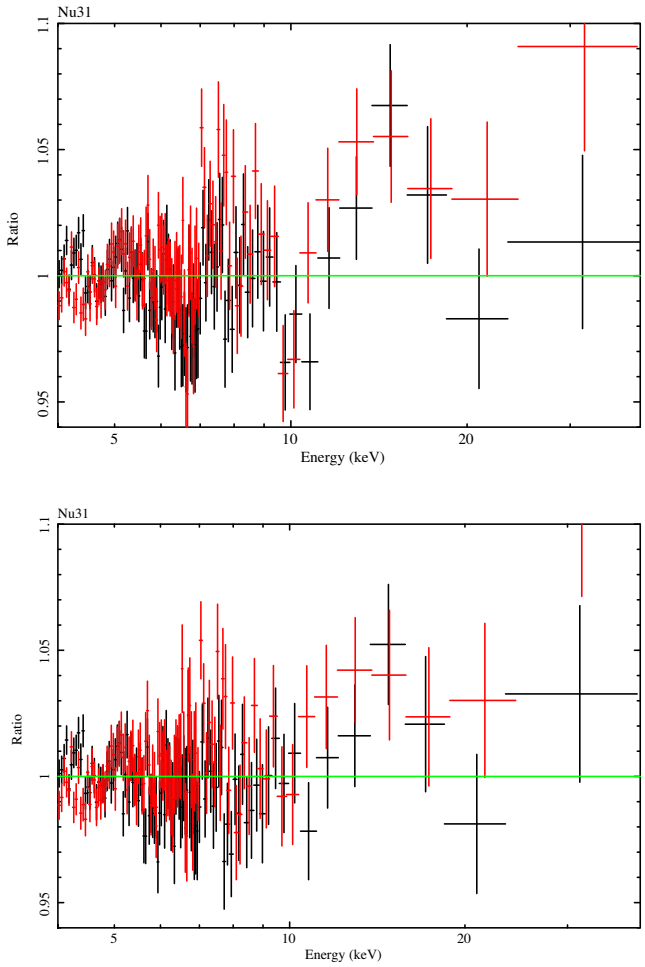

Figure 7. Top panel: ratio of Nu31 to the best-fitting model with `kerrbb` and `3kbb`. Bottom panel: as above but after Gaussian absorption at 6.6 keV and edge at 9.2 keV have been included in the fitted spectrum.

The standard Shakura & Sunyaev (1973) accretion disc assumes a zero-stress boundary condition at the ISCO. Matter enters ballistic plunge orbits at that radius with very little dissipation or further emission as it falls into the black hole. Later work in which the effect of magnetic fields is considered has suggested that stresses can and do occur at the ISCO, leading to dissipation and excess emission as matter enters the plunge region (Hawley & Krolik 2002; Machida & Matsumoto 2003; Shafee et al. 2008; Zhu et al. 2012; Abolmasov 2014). One of the most detailed studies by Zhu et al. (2012) shows that farther inward flow can cause a weak power-law-like continuum composed of ever hotter blackbody (bb) emission as matter falls further. Modelling the *NuSTAR* spectra as a disc blackbody together with three to four blackbodies (`diskbb + bb + bb + bb`) does give reasonable fits (e.g. Fig. 8).

Much as a waterfall produces chaos from a smooth stream, the flow from an accretion disc into the plunge region is expected to be highly variable (Hawley & Krolik 2002; Machida & Matsumoto 2003). We indeed find that the general disc emission varies little, but the emission above 6 keV is increasingly variable (Figs 9 and 10). For Nu27, the power-law component shows 25 per cent variability (including a significant drop throughout the observation), and for Nu29, it is 10 per cent. The rapid variability shown in the latter drops across the 6−10 keV band in a manner mid-way between that of the

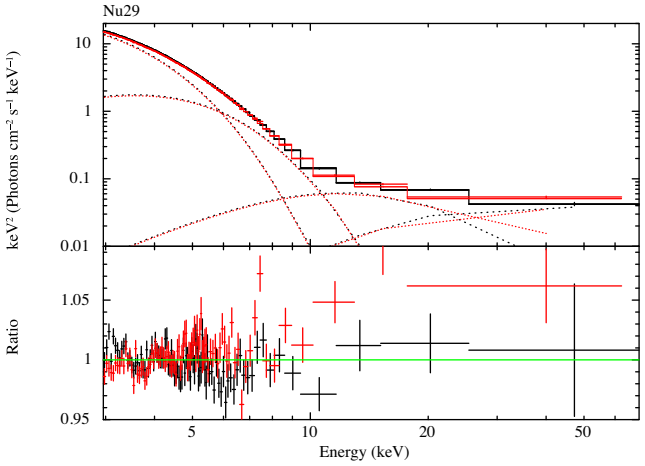

Figure 8. *NuSTAR* spectra of observation 29 with the hard tail fitted by two extra blackbody components.

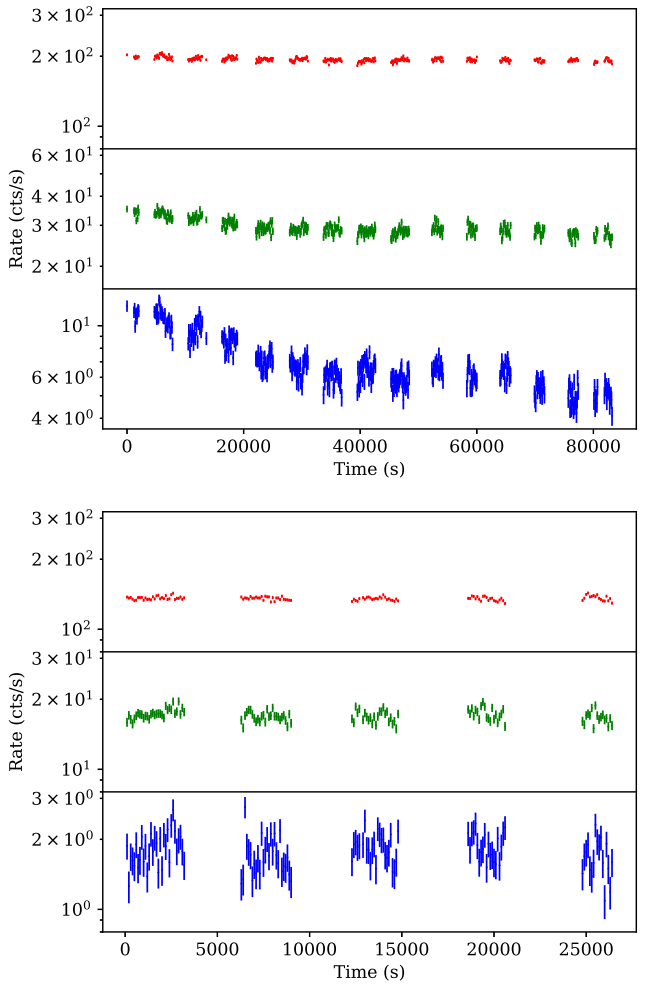

Figure 9. *NuSTAR* light curves of observations 27 (top panels) and 29 (bottom panels) in the energy bands 3–4, 6–8, and 10–78 keV. The bin size is 100 s.

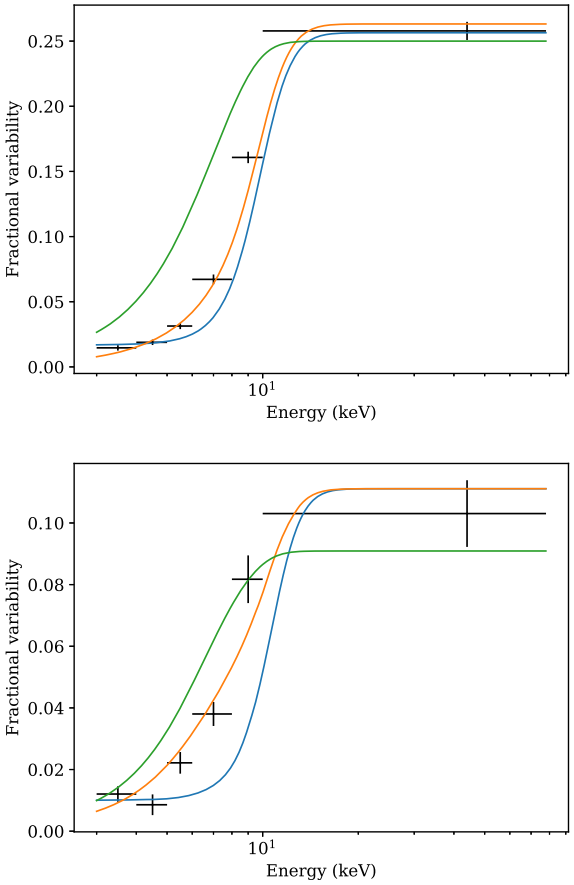

Figure 10. Fractional variability in observations 27 and 29. The solid lines show the expectation when the additional blackbody has the same amplitude as the disc (lower line), when the amplitude is freely fitted (middle line), and when it has the same amplitude as the power-law component (upper line).

power-law component and the disc. Further work on the variability is beyond the scope of this paper and will be reported elsewhere.

4 DISCUSSION

MAXI J1820+070 has been well observed by *NuSTAR* and *NICER* during the soft state of its bright outburst in 2018. The source peaked at an Eddington fraction of about 20 per cent before declining to about 10 per cent (assuming a blackhole mass of $8\,M_\odot$). Here we have examined the soft-state spectra and shown that, in addition to the usual disc-blackbody and power-law components, a further blackbody component is required. The flux of this extra component declines during the soft state from about 12 to 4 per cent of the flux of the disc component. A similar excess blackbody is required if a `kerrbb` model is used instead of `diskbb`.

A straightforward explanation for the excess is emission from the innermost part of the accretion flow across the ISCO, as the accreting matter begins to fall in the plunge region and then to the black hole. Magnetic stresses at the ISCO can delay the infall and power the emission. Modelling the luminosity and temperature of the excess blackbody through simulations should lead to further understanding of the strength and nature of the magnetic fields in the accretion disc around the ISCO.

Reflection could be involved, but is disfavoured by the large difference in the rate of change of the power-law component and the 6–10 keV excess. Any such reflection would also originate from the innermost part of the disc.

Zhu et al. (2012) show that the Thomson optical depth through the disc remains high within the beginning of the plunge region, so radiation has to diffuse out. Moreover, despite dropping inwards, the density remains high enough for the electrons and protons in the gas to be thermalized, so blackbody radiation is expected.

The effect of non-zero torque can be mimicked in `kerrbb` with the torque parameter η. Normally, this is set to zero, as has been the case so far here. If we allow η to be a free parameter and just fit `constant * (kerrbb + pco)` to the *NuSTAR* and *NICER* data of epoch 29, then the fit improves, reaching a χ^2 minimum about 400 more than when a bb is used. The residuals are reduced by about one half, but an excess remains in the 6–10 keV band. On discussion of `kerrbb`, Li et al. (2005) point out that the use of η will be only partially successful since the model assumes no emission within the ISCO, which is unlikely. The net result is to support our claim that the blackbody excess is associated with a non-zero torque, leading to excess emission both immediately outside and *inside* the ISCO.

The power-law component is not simple, but has a curvature, which we model with a cut-off. This improves the fit but leaves significant residuals. The component shows large variability of 10–25 per cent. The excess blackbody component shows variability intermediate between that of the power-law and the disc components (as expected, the disc itself shows little variability). The power-law component can also be modelled with a sequence of blackbody spectra (Fig. 8), which could originate in the plunging flow (see Zhu et al. 2012).

One question remains: Why is the 6–10 keV spectral component not commonly seen? First, we note that the effect may be small when the black hole spin is high and the plunge region relatively small due to the proximity of the ISCO to the event horizon of the black hole (see the discussion by Zhu et al. 2012). Secondly, the effect is quite subtle, requiring an accurate measurement of an excess flux of only 10 per cent in the 7–12 keV band. (Figs 4 and 5). Thirdly, a few sources do sometimes show high-temperature components requiring a small emitting region (e.g. Muno et al. 2001; Tomsick et al. 2005), although the overall situation of those sources is quite different from that studied here.

Finally, we note that Oda et al. (2019) have reported a similar excess in single-epoch *Suzaku* spectra of the black hole candidate MAXI J1828−249 taken during the intermediate state as the soft state was beginning. They explain it using separate Comptonization components, one of which accounts for the power-law tail and the other for the 5–10 keV excess. The latter is due to photons from either (a) the inner edge of the `diskbb`, which has a temperature similar to that seen in MAXI J1820+070, upscattered using `nthcomp` in an electron cloud of temperature 1.2 keV and optical depth $\tau > 3.5$, or (b) the whole disc with a cloud of temperature 14 keV and optical depth about unity. We find that model (a) gives a good fit to the epoch 29 *NICER* and *NuSTAR* data with $\tau \sim 25$ but is *very* sensitive to the electron temperature ($kT_e = 0.905^{+0.016}_{-0.021}$ keV). A visual comparison of the best-fitting `nthcomp` and `bb` spectra shows them to be almost indistinguishable above 3 keV, so from the *NuSTAR* point of view of fitting MAXI J1820+070, they can be considered equivalent. We suspect that the blackbody emission from the ISCO is also relevant to MAXI J1828−249.

We conclude that an excess blackbody component is the simplest explanation for the soft-state spectral behaviour of MAXI J1920+070 and identify that component with the start of the plunge region.

ACKNOWLEDGEMENTS

ACF and SD acknowledge support from European Research Council Advanced Grant FEEDBACK, and DRW is supported by NASA through Einstein Postdoctoral Fellowship grant number PF6-170160, awarded by the Chandra X-ray Center, operated by the Smithsonian Astrophysical Observatory for NASA under contract NAS8-03060.340442. CSR thanks the UK Science and Technology Facilities Council (STFC) for support under the New Applicant grant ST/R000867/1, and the European Research Council (ERC) for support under the European Union's Horizon 2020 research and innovation programme (grant 834203).

REFERENCES

Abolmasov P., 2014, MNRAS, 445, 1269
Buisson D. J. et al., 2019, MNRAS, 490, 1350
Gandhi P., Rao A., Johnson M. A. C., Paice J. A., Maccarone T., 2019, MNRAS, 485, 2642
Gendreau K. C. et al., 2016, in den Herder J.-W. A., Takahashi T., Bautz M., eds, Proc. SPIE Conf. Ser. Vol. 9905, The Neutron star Interior Composition Explorer (NICER): design and development. SPIE, Bellingham, p. 16
Hawley J. F., Krolik J. H., 2002, ApJ, 566, 164
Kara E. et al., 2019, Nature, 565, 198
Kawamuro T. et al., 2018, Astron. Telegram, 11399, 1
Li L., Zimmerman E. R., Narayan R., McClintock J. E., 2005, ApJS, 157, 335
Ludlam R. et al., 2018, ApJ, 858, L5
Machida M., Matsumoto R., 2003, ApJ, 585, 429
Makishima K., Maejima Y., Mitsuda K., Bradt H. V., Remillard R. A., Tuohy I. R., Hoshi R., Nakagawa M., 1986, ApJ, 308, 635
Matsuoka M. et al., 2009, PASJ, 69, 999
Matt G., Fabian A. C., Ross R. R., 1993, MNRAS, 262, 179
Muno M., Remillard R. A., Morgan E. H., Waltman E. B., Dhawan V., Hjellming R. M., Pooley G., 2001, ApJ, 556, 515
Oda S. et al., 2019, PASJ, 71, 108
Ponti G., Fender R. P., Begelman M. C., Dunn R. J. H., Neilsen J., Coriat M., 2012, MNRAS, 422, L11
Ross R. R., Fabian A. C., 2007, MNRAS, 381, 1697
Shafee R., McKinney J. C., Narayan R., Tchekhovskoy A., Gammie C. F., McClintock J. E., 2008, ApJ, 687, L25
Shakura N. I., Sunyaev R. A., 1973, A&A, 24, 337
Shappee B. J. et al., 2014, ApJ, 788, 48
Shidatsu M., Nakahira S., Murata K. L., Adachi R., Kawai N., Ueda Y., Negoro H., 2019, ApJ, 874, 173
Steiner J. F., Narayan R., McClintock J. E., Ebisawa K., 2009, PASJ, 121, 1279
Tomsick J. A., Corbel S., Goldwurm A., Kaaret P., 2005, ApJ, 630, 413
Torres M. A. P., Casares J., Jimenez-Ibarra F., Munoz-Darias T., Armas Padilla M., Jonker P. G., Heida M., 2019, ApJ, 882, L21
Tucker M. et al., 2018, ApJ, 867, L9
Zhu Y., Davis S. W., Narayan R., Kulkarni A. K., Penna R. F., McClintock J. E., 2012, MNRAS, 424, 2504
Zimmerman E., Narayan R., McClintock J. E., Miller J. M., 2005, ApJ, 618, 832
Zycki P., Czerny B., 1994, MNRAS, 266, 653

This paper has been typeset from a TEX/LATEX file prepared by the author.